

Interactive Effects of Span Length and Rafter Angle on The Ductility and Stability of Steel Warehouse Structures

Kevin C. Darmawana*, Budi Suswantoa, Aniendhita R. Amaliaa

Correspondence

^aDepartment of Civil Engineering, Sepuluh Nopember Institute of Technology, ITS Campus Sukolilo, Surabaya 60111, Indonesia.

Corresponding author email adress: kevincandradarmawan@gmail.com

Submitted : 14 January 2025 Revised : 15 June 2025 Accepted : 25 June 2025

Abstract

The warehouse frame is a specialized steel structure requiring more complex calculations than standard portal frames. This study investigates the impact of rafter angle and span length on ductility and stability. Results indicate that increasing span length enhances ductility but reduces stability due to higher story drift. For example, M1 (10-meter span) shows a ductility of 4.62 and story drift of 13.64 mm, while M3 (20-meter span) achieves 5.07 (+9.62%) with a drift of 46.77 mm. A larger rafter angle slightly increases ductility but decreases stability. M1 (10° angle) records 4.62 ductility and 13.64 mm drift, whereas M7 (20° angle) reaches 4.71 (+1.79%) with 16.92 mm drift. Higher structure stiffness reduces ductility but boosts stability. M3 (128.29 kN/m stiffness) shows 5.07 ductility and 46.77 mm drift, while M12 (192.67 kN/m) records 4.96 (-2.17%) with 29.68 mm drift. Despite M12's minor ductility reduction, M3 demonstrates better elastic-plastic behavior. These findings reveal a clear polarity between ductility and stability.

Keywords

Ductility, rafter angle, span length, stability, warehouse frame

INTRODUCTION

A warehouse frame is a specialized steel structure requiring more advanced calculations than rectangular portal frames, commonly employed in single-story industrial buildings. Each component, including rafters, columns, base plates, haunches, and stiffeners, is subjected to combined bending moments and axial compressive forces, contributing to the overall structural integrity. The design of these elements is load-specific, with rafter angles varying based on roofing materials [1]. The popularity of warehouse frames stems from their lightweight design and streamlined construction process, driving a growing demand for structural steel warehouses across various industries [2]. Structures must be engineered to balance both safety and economic efficiency. While adherence to prescriptive code regulations during the design process ensures structural safety, it may also introduce unnecessary financial burdens on stakeholders, potentially inflating project costs beyond essential requirements [3].

The carbon concentration in steel plays a pivotal role in determining its strength and ductility, which in turn significantly impacts the material's structural behaviour [4]. Steel with a carbon content below 2% is classified as low-carbon steel. Its combination of high strength and ductility is essential for designing lightweight structures that enhance overall structural safety and performance [5]. The use of steel in construction continues to advance due to its high strength. However, despite its strength, several factors must be considered in the design, including yield stress, ultimate stress, elastic modulus, shear modulus, Poisson's ratio, and coefficient of thermal expansion [6].

Structural engineers must account for a comprehensive range of design parameters, resulting in structures that are both economically efficient and resilient against dynamic loads and inherent uncertainties [7]. Moment-resistant steel frames are commonly used, especially in industrial buildings, due to their high resistance to seismic forces. This is primarily due to their excellent energy dissipation capacity and the structure's ductile behaviour [8]. The development of strategies to mitigate extensive damage in steel frame structures during seismic events or to expedite their post-earthquake functional recovery has become a critical focus within the field of structural engineering [9].

As the demand for post-earthquake reparability and rapid recovery of structures increases, significant research attention has been directed toward the development of earthquake-resilient systems designed to maintain continuous functionality even after seismic events [10]. Ductility is essential for ensuring the safety of a structure, as the lack of ductile behaviour can result in sudden and catastrophic structural failure [11]. High-strength, highductility low-carbon steels are critically needed to facilitate structural light-weighting and enhance overall structural safety [12]. In designing ductile steel structures, a ductile material can undergo significant inelastic deformation without losing its strength. In contrast, brittle behaviour refers to a material's tendency to fracture without plastic deformation. Among commonly used building materials, structural steel is the most ductile. A building can achieve a ductile response by avoiding brittle failure and employing design strategies that ensure effective energy dissipation mechanisms [13]. Energy dissipation mechanisms are employed to mitigate structural component damage during seismic events, enhancing the overall resilience and performance of the structure under dynamic loading conditions [14]. Moment frames are classified into three types based on their energy dissipation capacity: Ordinary Moment Frames (OMFs), Intermediate Moment Frames (IMFs), and Special Moment Frames (SMFs) are classified based on their ductility levels. OMFs have ductility values between 2.5 and 4.0, IMFs range from 4.5 to 6.0, while SMFs demonstrate ductility exceeding 6.0 [15]. One of the most critical failure mechanisms affecting structural performance during seismic events is the brittle fracture of structural members or their connections, which can severely compromise the overall integrity and seismic resilience of the system [16].

The stability of steel structures is assessed based on inelastic deformation induced by lateral loads. Nonlinear analyses, such as pushover and nonlinear time history analysis, are essential for determining the inelastic deformation. The AISC 341-16 [17] standard mandates stability analysis using second-order analysis, which incorporates the P-delta effect in evaluating structural stability. P-delta refers to the extra vertical load generated by the horizontal displacement of a structure. In secondorder analysis, this effect can be disregarded if the stability coefficient (Θ) is below 0.1 [18], a structure is deemed stable if the inter-story drift defined as the horizontal displacement between two consecutive floors relative to the story height remains below the allowable limit. The allowable drift is determined by a specified ratio, which varies depending on building codes and the type of structure. Ensuring that the actual drift does not exceed this allowable limit is crucial for maintaining both structural stability and safety. Incorporating an appropriate allowance for geometric imperfections is essential to ensuring structural stability. The traditional approach to designing steel structures follows a two-step process. First, internal stress resultants within the structure are calculated under design loads, typically through first- or second-order elastic analysis. Next, these stress resultants are compared with the design resistances of each structural element, which are derived from semi-empirical design formulas outlined in international standards. This approach implicitly accounts for geometric imperfections, but it may also involve simplifications or assumptions that do not fully capture the true behaviour of the structure [19].

An earthquake is an abrupt geophysical phenomenon characterized by its high randomness and unpredictability in both time and space, presenting a substantial risk to human life and property security [20]. Enhancing the resilience of existing structures in high-seismicity regions, especially those susceptible to poor performance during severe ground motions, presents a complex and vital challenge for structural engineers, demanding innovative and adaptive design solutions [21]. Progressive collapse in a structural system refers to a phenomenon where localized damage in individual components propagates through the system, ultimately resulting in the failure of the entire structure or significant portions thereof [22]. The structural response of steel members can be rigorously evaluated through geometrically and materially nonlinear analysis, incorporating the consideration of structural failure mechanisms [23]. Conventional seismic analysis methods outlined in design standards, such as the Equivalent Lateral Force (ELF) method and the Response Spectrum (RS) method, rely on linear assumptions, presuming that structural systems respond elastically to seismic forces. The ELF method simplifies the dynamic nature of seismic loads by converting them into equivalent static forces, while the RS method uses spectral curves to represent how structures respond across different ground motion frequencies. However, these linear approaches often lack the capacity to accurately reflect the complex nonlinear behaviours exhibited by structures during severe seismic events, such as plastic deformations, energy dissipation, and cumulative damage. In contrast, nonlinear time-history analysis provides a more robust and detailed evaluation by accounting for both material and geometric nonlinearities. This advanced analytical approach delivers a refined understanding of seismic responses, capturing essential phenomena such as nonlinear dynamic behaviour, localized structural failures, and progressive stiffness deterioration. By offering a realistic simulation of structural performance under extreme conditions, it significantly surpasses the predictive capabilities of traditional linear methods, making it invaluable for highrisk seismic design scenarios [24]. Time history analysis is used to assess the seismic response of a structure subjected to dynamic earthquake loading [25].

Structural steel, recognized for its superior strength-toweight ratio and remarkable ductility, is highly favored in seismic-resistant construction. When a structure's strength and deformation capacity is predominantly governed by the flexural behaviour of steel components, as in momentresisting frames, the most efficient mechanism for energy dissipation is the development of flexural plastic hinges in these elements. This localized inelastic response helps absorb and dissipate seismic energy, enhancing the structure's overall performance during seismic events. This targeted inelastic response not only enhances the structure's capacity to absorb and dissipate seismic energy but also significantly bolsters its overall resilience against seismic forces [26]. Preventing seismic collapse is a critical focus in both design and evaluation, serving as a fundamental requirement in seismic codes [27]. Nonlinear dynamic analysis is widely regarded as the most realistic and accurate method for seismic analysis. To obtain a reliable estimation of seismic response, it is essential to carefully select a well-curated set of ground motion records [28]. Steel-framed structures exhibit pronounced nonlinear behaviour due to the inherent plasticity of the material and the slenderness of their elements, making them a focal point for extensive research. This structural typology has served as a foundation for the initial development of many structural analysis software, providing a critical platform for advancing design methodologies and computational modeling techniques [29]. Pushover analysis is a simplified nonlinear technique used to estimate the dynamic demands placed on a structure during earthquake excitations. The initial step in this approximate method involves identifying the target displacement, which is the maximum roof movement, derived from the base shear versus roof displacement curve [30]. In pushover analysis, the configuration of plastic hinges within the structural framework is essential. Although the plastic hinge model is less precise than the plastic zone model, it offers greater



computational efficiency and practicality for assessing structural performance in standard engineering design applications. This model assumes that beam-column elements remain predominantly elastic, with inelastic deformations localized exclusively at the plastic hinge regions [31].

According to the research by G. S. Patil and Chougule (2020), a warehouse frame with an 80-meter span exhibits a horizontal deflection approximately of 25.13% greater and a vertical deflection of about 201.55% greater than a frame with a 20-meter span. This study highlights that the span length of a warehouse frame has a significant impact on both its horizontal and vertical deflections [32]. Additionally, research by Alan Scott Hoback and Naser Katanbafnezhad (2020) demonstrates that increasing the rafter angle in a gable frame leads to an increase in the stress ratio of the structure [33]. An essential aspect of optimal design involves creating a structure with proportionate geometry, such as selecting appropriate frame and column spacing and determining the roof slope based on the building's intended function. Improper structural design may lead to increased construction costs due to excessive material use, extended fabrication times, and higher labour expenses. Previous studies have not yet addressed the nonlinear behaviour of structures resulting from the combined effects of variations in rafter angle and span length on the ductility and stability of warehouse steel frames. Nonlinear analysis is integral to both the design and performance assessment of structures. By evaluating the ductility and stability of warehouse frames, a more comprehensive understanding of the structure's behaviour can be achieved, offering valuable guidance for more efficient planning.

RESEARCH SIGNIFICANCE

This study aims to investigate the combined effects of span length variation and rafter angle size on the ductility and stability of warehouse steel structures. In the analysis of span length and rafter angle variations, two structural configurations are considered: Type A and Type B. These configurations are distinguished by the dimensional specifications of the column and rafter section. Specifically, Type A employs an HB 300 column profile paired with a WF 300.200 rafter profile, whereas Type B utilizes an HB 350 column section in conjunction with a WF 350.250 rafter section. Both configurations are fabricated using ASTM A36 grade steel, ensuring material consistency. The primary distinction between Type A and Type B lies in the flange dimensions of the section, which inherently influence the cross-sectional area and moment of inertia. To evaluate the implications of these variations, span lengths and rafter angles are systematically altered to investigate their effects on structural ductility and stability. The detailed framework of the research model is delineated in Table 1. This study aims to investigate the combined effects of span length variation and rafter angle size on the ductility and stability of warehouse steel structures. It further seeks to examine the influence of using ductile and non-ductile cross-sections on the ductility and stability of these structures. The findings of this research are anticipated to provide valuable insights for the design of

steel warehouse structures with optimized ductility and stability behaviour.

Building on these considerations, this research focuses on three pivotal objectives: (1) assessing how variations in rafter angles influence structural ductility and stability, (2) exploring the impact of the span-to-height ratio (L/H) on the overall performance of ductility and stability, and (3) evaluating the distinct effects of structural Models A and B—characterized by differing stiffness properties—on ductility and stability. In light of the background and objectives presented, this study aspires to deliver several significant contributions. Firstly, it is intended to provide a substantive reference for design consultants in formulating steel warehouse structures with enhanced ductility and stability. Secondly, the research aims to enrich the academic discourse by advancing the understanding of ductile behavior and stability in steel warehouse structures, benefiting both the author and the academic community. The analysis is conducted exclusively through numerical methods, with no experimental validation undertaken. Additionally, the design of foundation systems is deliberately excluded from the parameters of this research. The hypothesis formulated for this research suggests that the span-to-height ratio (L/H) exerts a significant influence on the ductility and stability of the structure, whereas the effect of the rafter angle is comparatively less pronounced. Furthermore, it is hypothesized that structural stiffness serves as a critical determinant in enhancing the stability and ductility of steel structural systems. Several critical factors form the basis for drawing conclusions in this research, specifically the ductility of the structure influenced by variations in the rafter angle, span length, and joint stiffness. The ductility values corresponding to variations in rafter angle and span length are obtained through analysis using SAP 2000. Structural stability, on the other hand, is assessed by examining inelastic deformations induced by lateral loading. A structure is deemed stable if the inter-story displacement remains below the permissible inter-story displacement limit.

METHODOLOGY

This study seeks to investigate how the combination of span length variations and rafter angles influences the ductility and stability of steel warehouse structures. The methodology is designed to ensure a clear, structured approach, optimizing the accuracy and relevance of the results. In essence, the research involves modeling the steel warehouse structure using SAP 2000 software to conduct a detailed analysis. This research involves modeling the design of steel warehouse structures using Direct Analysis Method (DAM) in SAP 2000 software, with the output parameters including stress ratio, ductility, stability. Direct Analysis Method (DAM) constitutes a modern framework for evaluating the structural strength and stability of building systems, particularly steel frames. Unlike traditional design approaches that employ simplified assumptions, DAM offers a more rigorous representation of structural behavior by explicitly accounting for critical factors influencing performance. This study using SAP 2000 to incorporates the effects of P-Delta, material nonlinearity (including residual stresses arising from the hot-rolled process), and inelastic behavior through the



application of reduced stiffness as fundamental components of the Direct Analysis Method to achieve a more accurate evaluation of the structural response.

Three warehouse types are designed with areas of 360 m², 540 m², and 720 m², using three structural height-to-span ratios (L/H): 1, 1½, and 2. The warehouses are intended for production goods storage, with pallet racks measuring H.250 cm x L.230 cm and a capacity of 1 ton per pallet, arranged to reach a total rack height of 7.5 meters. Consequently, the column height for all types is fixed at 10 meters. The spans are set at 10, 15, and 20 meters, with rafter angle variations of 10°, 15°, and 20°. The study will assess the impact of L/H ratio and rafter angle variations on ductility and stability. The resulting values will be compared to evaluate how these factors influence structural performance. The variations in the study are summarized in Table 1.

Table 1 The variations in the study from the combination

of the L/H ratio and rafter angle size						
Model	Column	Rafter	Rafter angle	L/H ratio		
M1				1,0		
M2	_		$10^{\rm o}$	1,5		
M3	_			2,0		
M4	- HB	WF		1,0		
M5	300.300.	300.200	15°	1,5		
M6	11.17	.8.12		2,0		
M7	_	_		1,0		
M8	_		$20^{\rm o}$	1,5		
M9	_			2,0		
M10				1,0		
M11	_		$10^{\rm o}$	1,5		
M12	- - HB	WF -		2,0		
M13	350.350.	350.250		1,0		
M14	12.19	.8.12	15°	1,5		
M15	_			2,0		
M16	_	-		1,0		
M17	_		20°	1,5		
M18	_			2,0		

|--|

WF 300.200.8.12			Н	B 300.300.11	.17
ht =	294	mm	ht =	304	mm
bf =	200	mm	bf =	301	mm
tw =	8	mm	tw =	11	mm
tf =	12	mm	tf =	17	mm
r =	18	mm	r =	18	mm
A =	7238	mm ²	A =	13480	mm ²
Ix =	11300	cm ⁴	Ix =	23400	cm ⁴
Iy =	1600	cm ⁴	Iy =	7730	cm ⁴
rx =	125	mm	rx =	132	mm
ry =	47,1	mm	ry =	75,7	mm
Sx =	771000	mm ³	Sx =	1540000	mm ³
Sy =	160000	mm ³	Sy =	514000	mm ³
Zx =	822600	mm^3	$\mathbf{Z}\mathbf{x} =$	1669054	mm^3

Table 3 Detail of Section for model B						
F 350.250.8.	12	Н	B 350.350.12	.19		
336	mm	ht =	350	mm		
249	mm	bf =	350	mm		
8	mm	tw =	12	mm		
12	mm	tf =	19	mm		
20	mm	r =	20	mm		
8815	mm ²	A =	17390	mm ²		
18500	cm ⁴	Ix =	40300	cm ⁴		
3090	cm ⁴	Iy =	13600	cm ⁴		
145	mm	rx =	152	mm		
59,2	mm	ry =	88,4	mm		
1100000	mm ³	Sx =	2300000	mm ³		
248000	mm ³	Sy =	776000	mm ³		
1162800	mm ³	Zx =	2493182	mm ³		
	F 350.250.8. 336 249 8 12 20 8815 18500 3090 145 59,2 1100000 248000	F 350.250.8.12 336 mm 249 mm 8 mm 12 mm 20 mm 8815 mm² 18500 cm⁴ 3090 cm⁴ 145 mm 59,2 mm 1100000 mm³ 248000 mm³	F 350.250.8.12 H 336 mm ht = 249 mm bf = 8 mm tw = 12 mm ff = 20 mm r = 8815 mm² A = 18500 cm⁴ Ix = 3090 cm⁴ Iy = 145 mm rx = 59,2 mm ry = 1100000 mm³ Sx = 248000 mm³ Sy =	F 350.250.8.12 HB 350.350.12 336 mm ht = 350 249 mm bf = 350 8 mm tw = 12 12 mm tf = 19 20 mm r = 20 8815 mm² A = 17390 18500 cm⁴ Ix = 40300 3090 cm⁴ Iy = 13600 145 mm rx = 152 59,2 mm ry = 88,4 1100000 mm³ Sx = 2300000 248000 mm³ Sy = 776000		

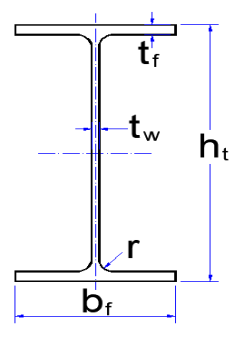


Figure 1. I-section

details:

I : moment of inertia
r : radius corner
r_{x,y} : radius of gyration
s_{x,y} : modulus of section
Z : plastic modulus

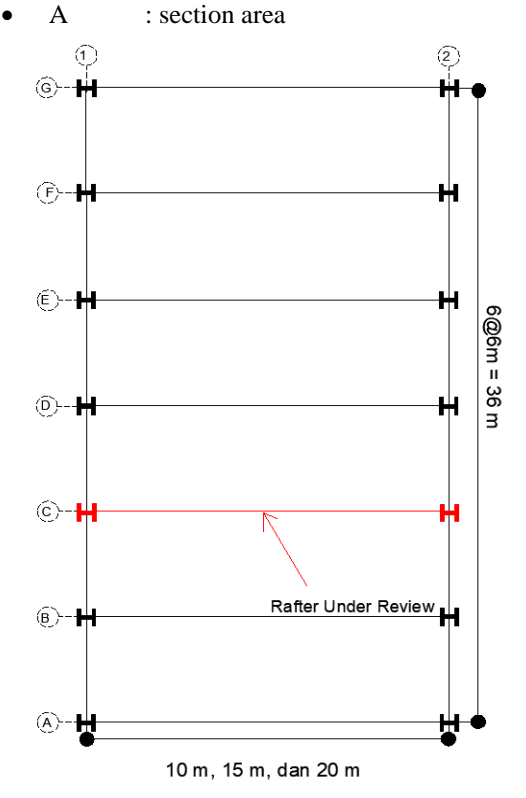


Figure 2. Floor Plan

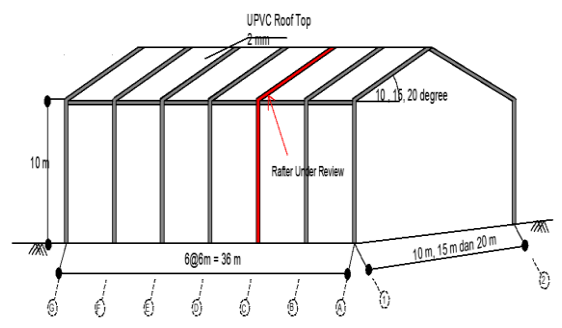


Figure 3. The structure in 3D

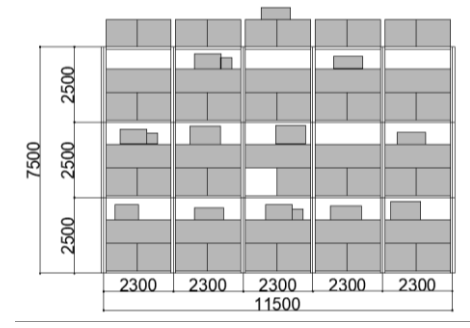


Figure 4. Pallet Racks

This study employs two column variations: HB 300.300.11.17 and HB 350.350.12.19, and two rafter variations: WF 300.200.8.12 and WF 350.250.8.12. All column and rafter section are fabricated from ASTM A36 steel. The column height for both variations is fixed at 10 meters. The column and rafter section will be analyzed to classify them as ductile or non-ductile sections based on AISC 341-16 standards, with the results presented in Table 5.

Table 4 Width-to-thickness ratio

rable 4 widul-to-thickness ratio							
Steel profile]	Flang	e	Web			
	λf		λd	λw		λd	
WF	8,33	<	9,23	33,75	<	59,08	
300.200.8.12							
WF	10,38	>	9,23	39,00	<	59,11	
350.250.8.12							
HB	8,85	<	9,24	24,55	<	58,79	
300.300.11.17							
HB	9,21	<	9,42	26,00	<	59,87	
350.350.12.19							

Table 5 Steel Profile ductility

Table 5 Steel Frome ductinty							
Steel profile	Flange	Web					
HB 300.300.11.17	ductile	ductile					
HB 350.350.12.19	ductile	ductile					
WF 300.200.8.12	ductile	ductile					
WF 350.250.8.12	non-ductile	ductile					

The structure is subjected to dead loads, super dead loads (2mm UPVC rooftop at 4.56 kg/m²), rain loads, roof live loads, and wind loads, in accordance with ASCE 7-22 [34]. Additionally, earthquake loads are considered, including nonlinear dynamic loads analyzed using Nonlinear Time History Analysis (NLTHA) and nonlinear static loads analyzed via pushover analysis. The spectral earthquake data for the NLTHA includes the Kobe, Coyote, and Tohoku earthquakes, adjusted to align with the response

spectrum of the research site in Nusantara City, East Kalimantan, Indonesia. NLTHA and pushover analyses are conducted for various L/H ratio and rafter angle combinations using SAP2000 software.

Dead load refers to the permanent, static force exerted on a structural system throughout its lifespan. This load encompasses the total self-weight of the structure, which is systematically computed through automated analysis using SAP 2000 software. The rain load imposed on the structure is transferred to the rafters as a uniformly distributed load. The load estimation adheres to the provisions of ASCE 7-22, yielding a calculated rain load of 0.245 kN/m². The wind load for this structure is determined utilizing the Main Wind Force Resisting System (Directional Procedure). Based on 2022 data from the Meteorology, Climatology, and Geophysics Agency, the recorded wind speed at the study site is 43 knots. According to ASCE 7-22, the live load on the roof is determined to be 0.96 kN/m². The live load will be modified according to the relevant reduction guidelines specified in the design standards.

The load combinations are based on AISC 360-16, which include dead load (D), super dead load (SDL), live load (L), wind load (W), and earthquake load (E), using the Load and Resistance Factor Design (LRFD) approach.

- 1. 1,4 D + 1,4 SDL
- 2. 1,2 D + 1,2 SDL + 1,6 L
- 3. 1.2 D + 1.2 SDL + (1.0 L or 0.5 W)
- 4. 1.2 D + 1.2 SDL + 1.0 W + 1.0 L
- 5. 0.9 D + 0.9 SDL + 1.0 W
- 6. 1.2 D + 1.2 SDL + 1.0 E + 1.0 L
- 7. 0.9 D + 0.9 SDL + 1.0 E

Additionally, load combinations accounting for the effects of seismic loads are applied, in accordance with AISC 341-16.

Table 6 Earthquake data

Tuote o Zurinquine dutu							
Number	Earthquake	Location	Time	Magnitude			
1	Coyote	Coyote,	1979	5,7			
		USA					
2	Kobe	Kobe,	1995	6,9			
		Jepang					
3	Tohoku	Tohoku,	2011	9,1			
		Jepang					

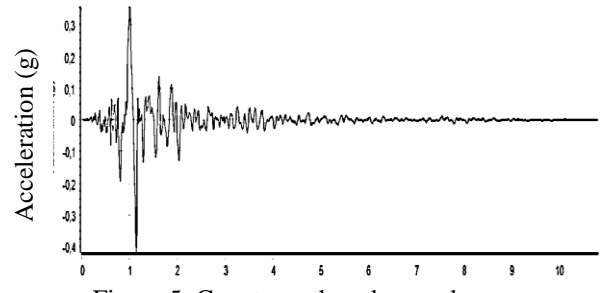


Figure 5. Coyote earthquake accelerogram

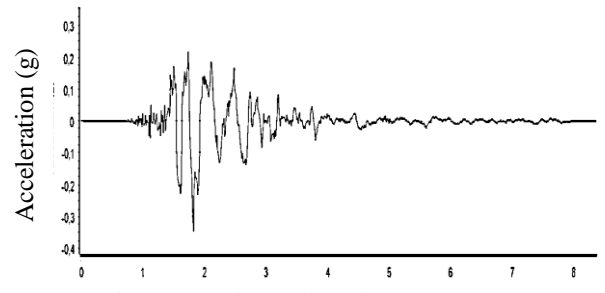


Figure 6. Kobe earthquake accelerogram



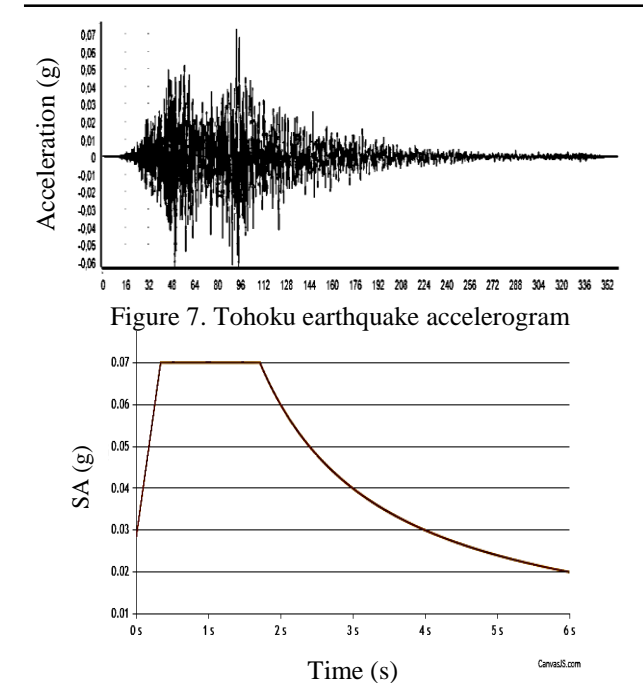


Figure 8. Nusantara spectrum response

• SS : 0.0692 g • S1 : 0.0753 g

RESULTS AND DISCUSSIONS

The span length and rafter angle variations are categorized into two structural types: Type A and Type B, distinguished by the cross-sectional section of their columns and rafters. Type A utilizes an HB 300 column section paired with a WF 300.200 rafter section, whereas Type B incorporates an HB 350 column section with a WF 350.250 rafter section. Both configurations employ ASTM A36 steel, ensuring consistent material properties across both types. To evaluate the influence of span length and rafter angle on the structural ductility and stability, Type A and Type B systematically configurations are varied. comprehensive framework of the research model is presented in Table 1, providing detailed information on the structure and parameters used in the analysis. The structural response to these variations is assessed through pushover analysis and Nonlinear Time History Analysis (NLTHA) using SAP 2000 software.

A. Model A - HB 300 and WF 300.200

Flexural performance assessment of the rafter profiles in steel warehouse structures is essential to ensure structural stability and load-bearing capacity. This evaluation aims to mitigate the risk of excessive deformation and structural failure, thereby safeguarding the occupants and maintaining the structural integrity under various loading conditions.

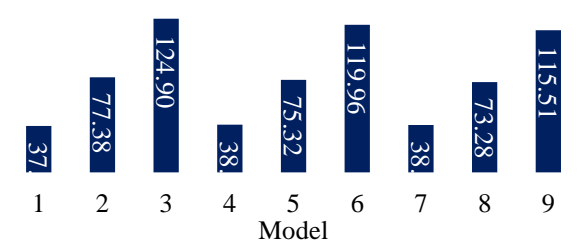


Figure 9. Flexural control of the rafter for Model A

All rafters in the Type A test model demonstrate adequate flexural capacity, as their ultimate moment (Mu) remains below the nominal moment capacity (ϕ Mn) of 177.68 kN.m, ensuring structural compliance with flexural performance criteria. Evaluating the shear capacity of rafter section in steel warehouse structures is essential to prevent failure caused by shear forces, which can lead to significant deformation. This assessment is critical for preserving the overall stability of the structure and ensuring its resilience under shear loads.

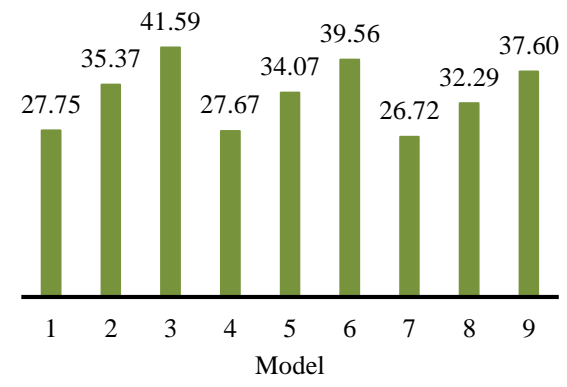


Figure 10. Shear control of the rafter for Model A All rafters in Model A demonstrate satisfactory shear performance, as their ultimate shear force (Vu) remains below the nominal shear capacity (ϕ Vn) of 311.04 kN/m, ensuring compliance with shear resistance criteria.

The rafters and columns in all Model A types exhibit a stress ratio value of less than 1.00, indicating that all models are in a safe condition, with the stress in the rafters remaining within the permissible limits. The Strong Column Weak Beam (SCWB) concept is a structural design principle that ensures columns can withstand greater loads than beams. Its purpose is to ensure that, in the event of failure, beams deform first, allowing columns to remain intact and providing time for evacuation. Additionally, SCWB enhances structural stability. The concept and calculation criteria are based on AISC 358-20. A structure satisfies the SCWB criteria when the ratio of the column's nominal bending strength to the beam's nominal bending strength at the plastic hinge exceeds 1.0. All Model A configurations exhibit an SCWB value greater than 1.0, confirming compliance with SCWB design requirements. The controlling of model A is presented in Table 7.

Table 7. Stress ratio of model A.

	Stress Ratio				
Model	Column		Raf	ter	
M1	0.121	< 1,00	0.216	< 1,00	
M2	0.239	< 1,00	0.443	< 1,00	
M3	0.377	< 1,00	0.713	< 1,00	
M4	0.126	< 1,00	0.223	< 1,00	
M5	0.238	< 1,00	0.432	< 1,00	
M6	0.366	< 1,00	0.687	< 1,00	
M7	0.127	< 1,00	0.224	< 1,00	
M8	0.173	< 1,00	0.422	< 1,00	
M9	0.356	< 1,00	0.663	< 1,00	



Table 8. SCWB analysis of model A							
Model	Mpc (kN.m)	Mpb (Kn.m)	SC	WB			
M1	412,142	397,036	1,038	>1,00			
M2	394,313	374,810	1,052	>1,00			
M3	393,383	372,083	1,057	>1,00			
M4	395,302	380,831	1,038	>1,00			
M5	394,293	374,384	1,053	>1,00			
M6	393,274	371,568	1,058	>1,00			
M7	395,230	380,032	1,040	>1,00			
M8	394,234	373,729	1,055	>1,00			
M9	409,808	386,212	1,061	>1,00			

Pushover analysis is performed to evaluate the seismic performance and capacity of the structure under progressively increasing lateral loads until failure occurs. The backbone curve used in this analysis is based on Table 9.6 of ASCE 41-13, representing the force-deformation relationship in structural elements as plastic hinges form. The following is the results of the pushover analysis for model A.

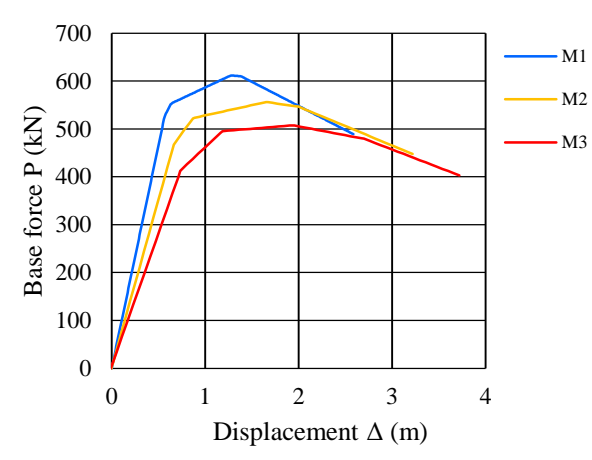


Figure 11. The pushover curves for M1, M2, and M3.

Figure 11 presents the pushover curves for models M1, M2, and M3, which share a rafter angle of 10° but differ in L/H ratios of 1, $1\frac{1}{2}$, and 2, respectively. The results indicate that the L/H ratio significantly influences the ultimate displacement (Δu) of the structure. Model M1, with an L/H ratio of 1, shows $\Delta u = 2.59$ m; M2, with L/H = $1\frac{1}{2}$, shows $\Delta u = 3.27$ m; and M3, with L/H = 2, shows $\Delta u = 3.72$ m. This suggests that the L/H ratio affects the length of the pushover curve, thereby affecting the structure's ductility.

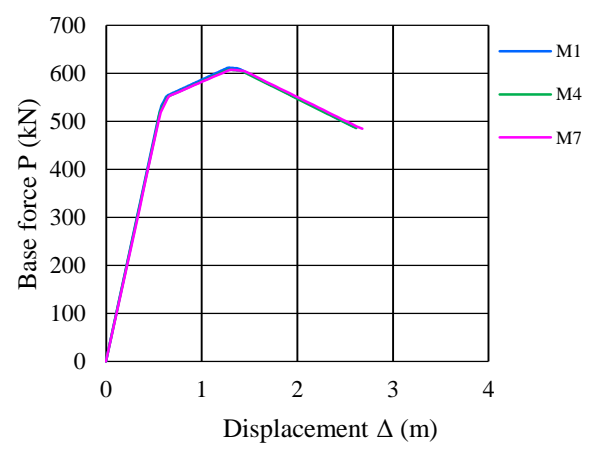


Figure 12. The pushover curves for M1, M4, and M7

Figure 12 presents the pushover curves for models M1, M4, and M7, all with an L/H ratio of 1 but differing rafter angles of 10° , 15° , and 20° , respectively. The analysis indicates that variations in the rafter angle have a minimal effect on the ultimate displacement (Δu) of the structure. Model M1, with a 10° rafter angle, shows $\Delta u = 2.59$ m; M4, with 15° , shows $\Delta u = 2.61$ m; and M7, with 20° , shows $\Delta u = 2.68$ m. The ultimate displacement (Δu) remains largely unchanged across these variations. The following is the pushover curves for all Model A configurations.

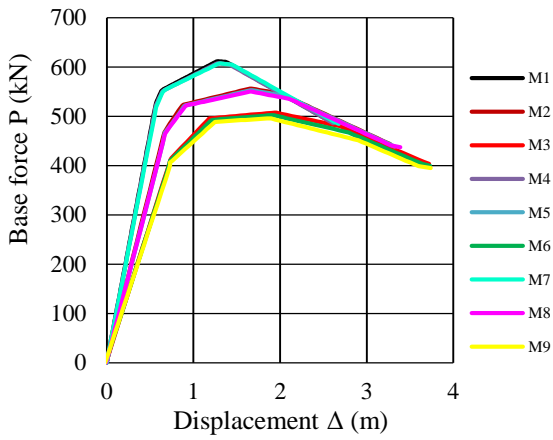


Figure 13. The pushover curves for model A

Non-linear time history analysis (NLTHA) is essential for evaluating structural stability. The following is the NLTHA results for Model A.

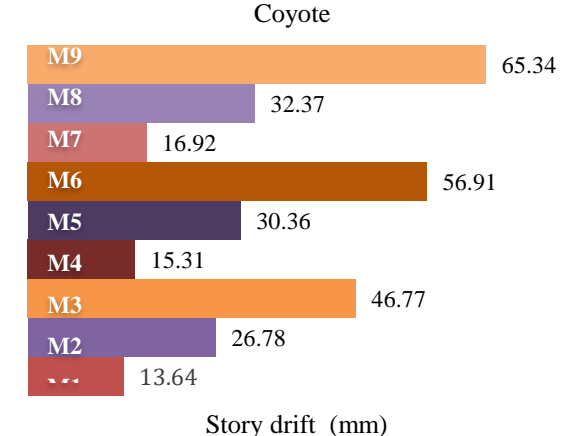


Figure 14. The story drift for model A (Coyote)

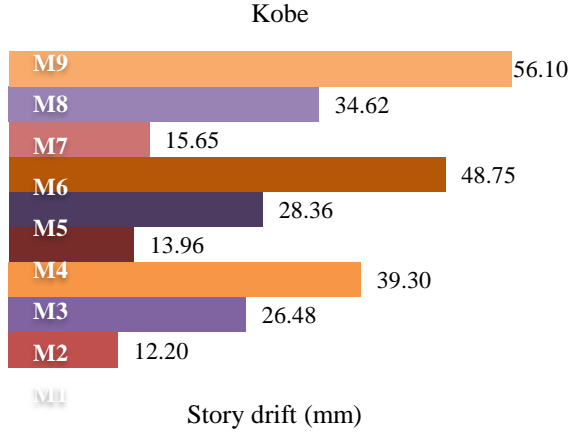


Figure 15. The story drift for model A (Kobe)

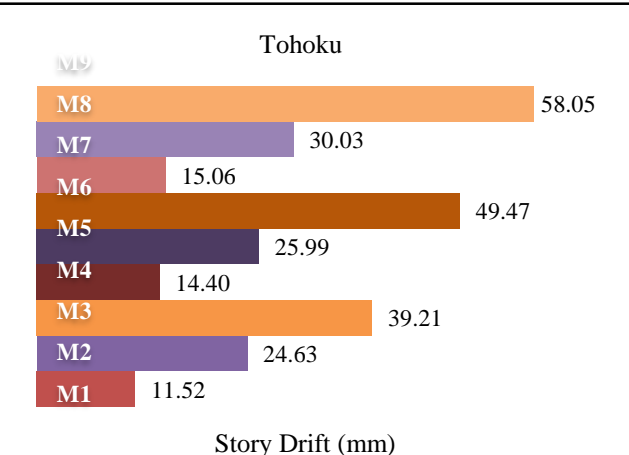


Figure 16. The story drift for model A (Tohoku)

The story drift (δ) values are derived from the displacements obtained through NLTHA. As shown in Table 4, an increase in the L/H ratio results in a higher story drift (δ), which subsequently impacts structural stability. For comparison, models M1, M2, and M3, all with a 10° rafter angle but varying L/H ratios of 1, 1½, and 2, respectively, were analyzed for the Coyote Earthquake. Model M1 shows a story drift (δ) of 13.64 mm, M2 shows 26.78 mm (a 96.33% increase), and M3 shows 46.77 mm (a 242.88% increase). The variation in rafter angle has a negligible impact on the story drift (δ) values. For comparison, models M1, M4, and M7, all with an L/H ratio of 1 but differing rafter angles of 10°, 15°, and 20°, respectively, were analyzed for the Coyote Earthquake. Model M1 exhibits a story drift (δ) of 13.64 mm, M4 shows 15.31 mm (a 12.24% increase), and M7 shows 16.92 mm (a 24.05% increase). Significant increases in story drift (δ) can compromise structural stability, hence it must remain below the allowable limit. With an allowable drift (Δa) of 200 mm, all models (M1 through M9) maintain story drift (δ) values below this threshold, confirming compliance with permissible limits.

The NLTHA results provide the story drift (δ) values for model A. Structural stability analysis is essential for ensuring the safety of the structure, particularly under earthquake loading. A structure is deemed stable if the stability coefficient (Θ) is lower than the maximum allowable stability coefficient (Θ max).

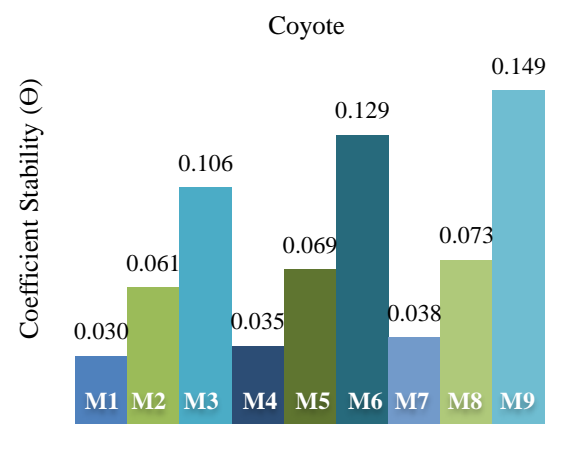


Figure 17. Coefficient Stability for model A (Coyote)

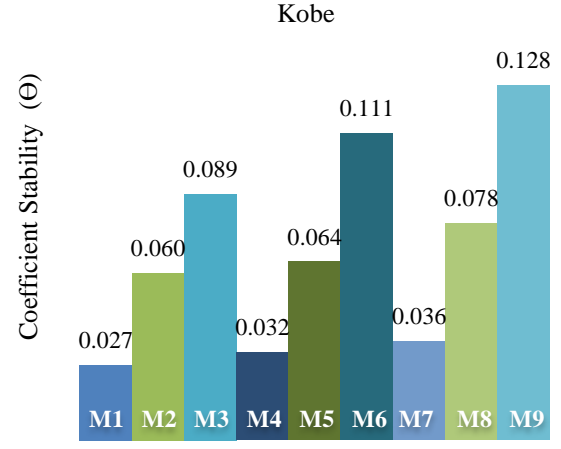


Figure 18. Coefficient Stability for model A (Kobe)

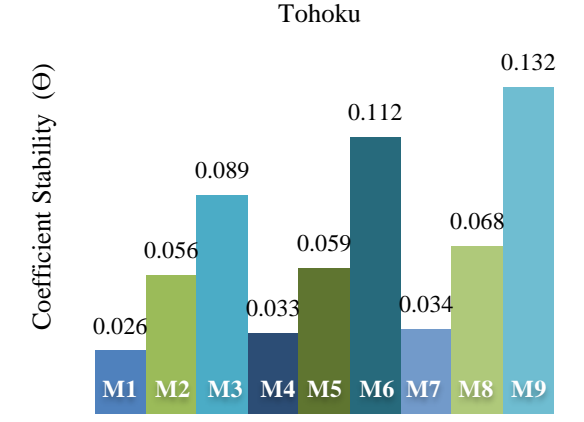


Figure 19. Coefficient Stability for model A (Tohoku)

Figure 17-19 demonstrates that all Model A configurations exhibit stability for the three earthquake scenarios, as their stability coefficient (Θ) values are below the maximum allowable threshold (Θ max = 0.167). The stability coefficient follows the trend M3 > M2 > M1, indicating that an increased L/H ratio enhances the structure's stability coefficient, consistent with the story drift (δ) analysis. For example, under the Coyote Earthquake, M1 has a stability coefficient (Θ) of 0.030, M2 has 0.061 (an increase of 103.3%), and M3 has 0.106 (an increase of 253.33%). In contrast, varying the rafter angle has a negligible effect on the stability coefficient. For instance, M1 has 0.030, M4 has 0.035 (a 16.67% increase), and M7 has 0.038 (a 26.67% increase). This trend aligns with the story drift values for Models M1 to M9, where increased story drift correlates with a higher stability coefficient, suggesting potential instability. The stability coefficient (Θ) and story drift (δ) are also influenced by structural stiffness, determined through modal analysis in SAP 2000. M1 has a stiffness of 179.16 kN/m, M2 has 149.06 kN/m, and M3 has 128.29 kN/m. Thus, increasing the L/H ratio reduces stiffness, leading to higher story drift and stability coefficients, which adversely affect structural stability.

Ductility analysis is crucial for assessing the failure behaviour of a structure, ensuring it does not get sudden collapse under seismic loading. The following is the ductility values for the structures in model A.

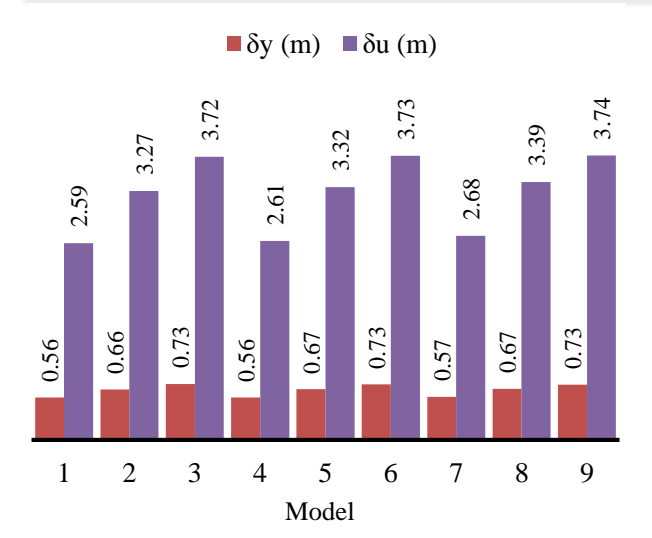


Figure 20. Yield and ultimate displacement for model A

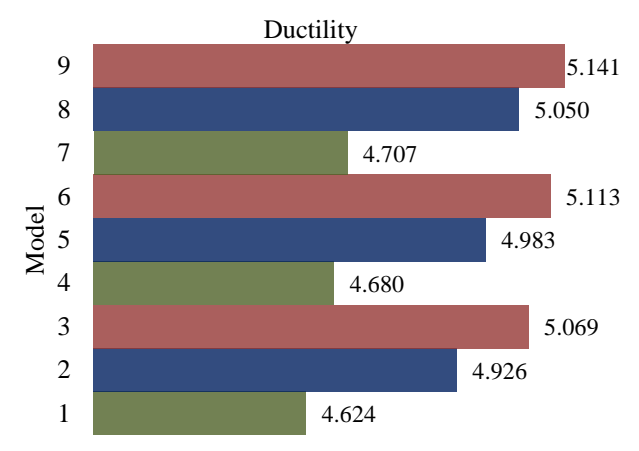


Figure 21. The ductility of model A

Figure 21 shows that Models M1 through M9 exhibit ductility values ranging from 4.5 to 6.0, classifying all Model A structures as Intermediate Moment Frames (IMF). In Models M1, M2, and M3, ductility increases with varying L/H ratios (1, 1½, and 2), while the rafter angle remains constant at 10°. Model M1 has a ductility value of 4.624, Model M2 has a value of 4.926 (an increase of 6.53% from M1), and Model M3 has a value of 5.069 (an increase of 9.62% from M1). The results indicate that a higher L/H ratio leads to increased ductility due to reduced stiffness, which consequently increases story drift (δ) and flexibility. This enhanced flexibility results in greater plastic deformation, as observed in the pushover curves. However, careful monitoring of stiffness reduction is necessary to prevent excessive flexibility that may lead to structural instability. This is addressed through the control of story drift (δ) and stability coefficient (Θ). In models M1, M4, and M7, the ductility of the structure shows a slight increase. These models, all with an L/H ratio of 1, differ in rafter angles of 10°, 15°, and 20°, respectively. Model M1 exhibits a ductility value of 4.624, M4 shows 4.680 (a 1.21% increase from M1), and M7 demonstrates 4.707 (a 1.79% increase from M1). While increasing the rafter angle improves the structure's ductility, the effect is marginal. This minor increase in ductility correlates with the relatively small changes in story drift (δ) and structural stiffness. In conclusion, steeper rafter angles marginally enhance the structure's ductility.

B. Model B – HB 350 and WF 350.250

Assessing the flexural performance of rafter profiles in steel warehouse structures is crucial for ensuring structural stability and load-bearing capacity. This evaluation helps prevent excessive deformation and potential structural failure, thereby protecting occupants and preserving the integrity of the structure under different loading scenarios.

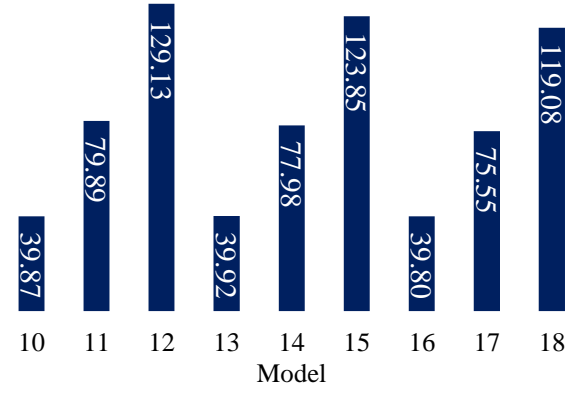


Figure 22. Flexural control of the rafter for Model B All rafters in Model B are considered safe under flexural conditions, as their ultimate moment (Mu) is lower than the nominal moment (ϕ Mn) of 251.16 kN.m. Shear capacity assessment of the rafter section in steel warehouse structures is critical to prevent collapse caused by shear forces, which can lead to excessive deformation, while also ensuring the overall stability of the structure.

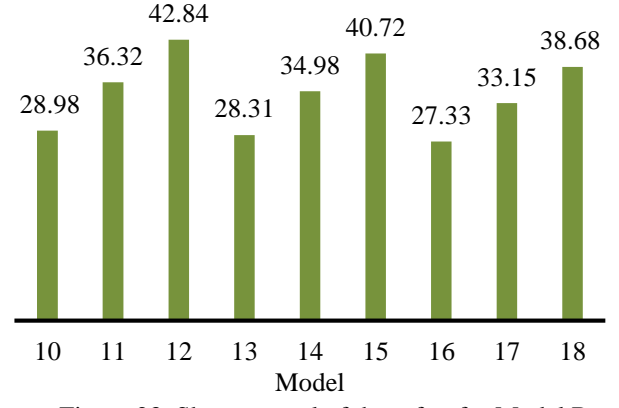


Figure 23. Shear control of the rafter for Model B It can be affirmed that all rafters in Model B exhibit adequate shear performance, as their ultimate shear force (Vu) remains below the nominal shear capacity (ϕ Vn) of 359.42 kN, ensuring compliance with shear resistance criteria.

Table 8. Stress ratio of model B

	Stress Ratio					
Model _	Column		Raft	er		
M10	0.085	<1,00	0.162	<1,00		
M11	0.165	<1,00	0.324	<1,00		
M12	0.261	<1,00	0.523	<1,00		
M13	0.087	<1,00	0.163	<1,00		
M14	0.162	<1,00	0.317	<1,00		
M15	0.253	<1,00	0.503	<1,00		
M16	0.088	<1,00	0.163	<1,00		
M17	0.159	<1,00	0.308	<1,00		
M18	0.246	<1,00	0.485	<1,00		



Table 9. SCWB analysis of model B						
Mpc (kN.m)	Mpb (kN.m)	SC	:WB			
616,669	565,267	1,091	>1,00			
590,454	531,581	1,111	>1,00			
589,326	526,734	1,119	>1,00			
591,648	541,957	1,092	>1,00			
590,418	530,971	1,112	>1,00			
589,196	526,025	1,120	>1,00			
591,562	540,711	1,094	>1,00			
590,356	530,023	1,114	>1,00			
589,010	525,202	1,121	>1,00			
	Mpc (kN.m) 616,669 590,454 589,326 591,648 590,418 589,196 591,562 590,356	Mpc (kN.m) Mpb (kN.m) 616,669 565,267 590,454 531,581 589,326 526,734 591,648 541,957 590,418 530,971 589,196 526,025 591,562 540,711 590,356 530,023	Mpc (kN.m) Mpb (kN.m) SC 616,669 565,267 1,091 590,454 531,581 1,111 589,326 526,734 1,119 591,648 541,957 1,092 590,418 530,971 1,112 589,196 526,025 1,120 591,562 540,711 1,094 590,356 530,023 1,114			

All rafters and columns in model type B exhibit a stress ratio of less than 1.0, signifying that the models are structurally safe. Furthermore, the SCWB values exceed 1.0, ensuring that all models comply with the SCWB building criteria. The following are the results of the pushover analysis for model B.

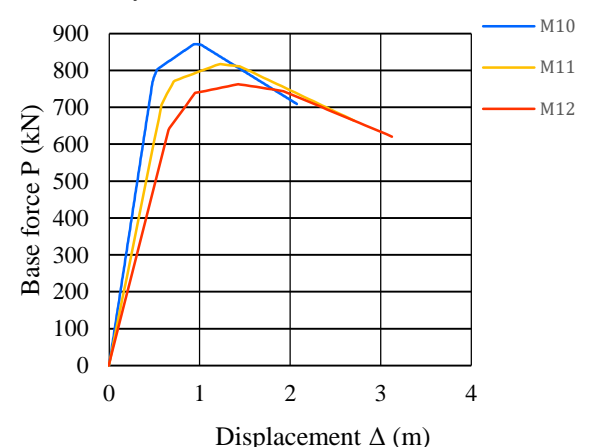


Figure 23. The pushover curves for M10, M11, and M12

Figure 23 illustrates the pushover curves for models M10, M11, and M12. These models, with identical rafter angles of 10° , exhibit varying L/H ratios of 1, $1\frac{1}{2}$, and 2, respectively. The data indicate that the L/H ratio significantly influences the ultimate displacement (Δu) of the structure. Specifically, Model M10 (L/H = 1) exhibits a Δu of 2.15 m, M11 (L/H = $1\frac{1}{2}$) shows a Δu of 2.81 m, and M12 (L/H = 2) demonstrates a Δu of 3.24 m.

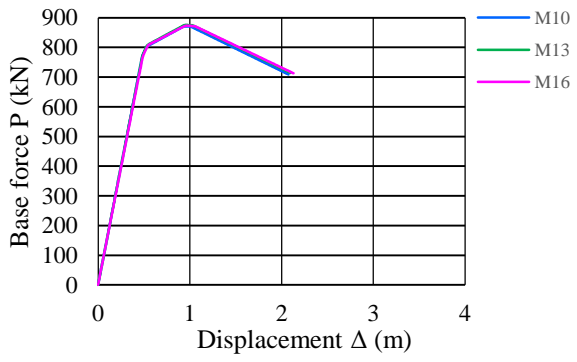


Figure 24. The pushover curves for M10, M13, and M16

Models M10, M13, and M16, each with an identical L/H ratio of 1, differ in rafter angles: 10° , 15° , and 20° , respectively. The pushover curves in Figure 4.19 indicate that variations in rafter angle exert negligible influence on the ultimate displacement (Δu). Specifically, Model M10

exhibits a Δu of 2.15 m, Model M13 a Δu of 2.19 m, and Model M16 a Δu of 2.23 m. These findings suggest that rafter angle adjustments have an insignificant effect on the ultimate displacement (Δu). The following is the pushover curves for all Model B configurations.

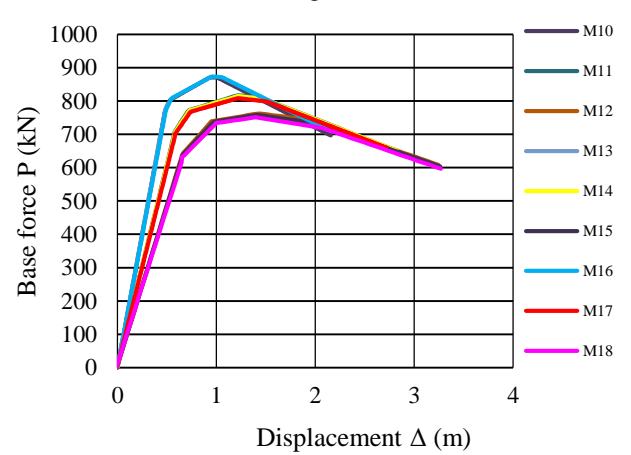


Figure 25. The pushover curves for model B

Non-linear time history analysis (NLTHA) is essential for evaluating structural stability. The following is the NLTHA results for Model B.

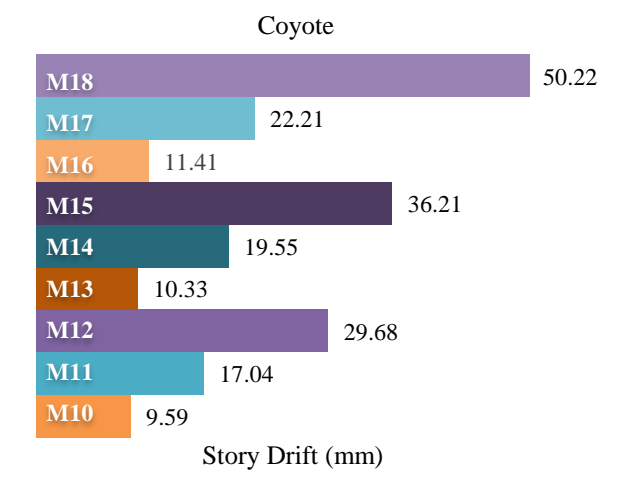


Figure 26. The story drift for model B (Coyote)

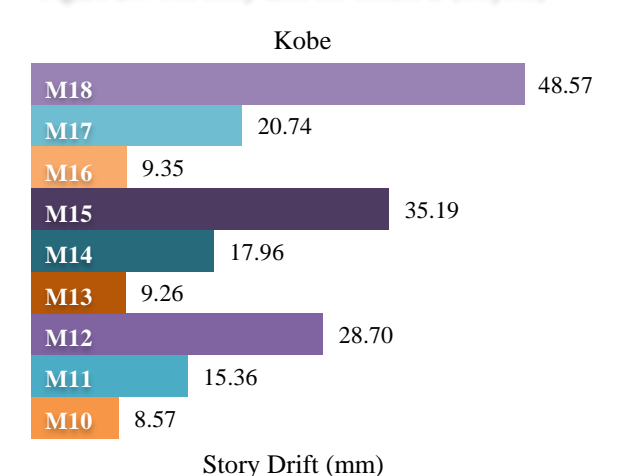


Figure 27. The story drift for model B (Kobe)



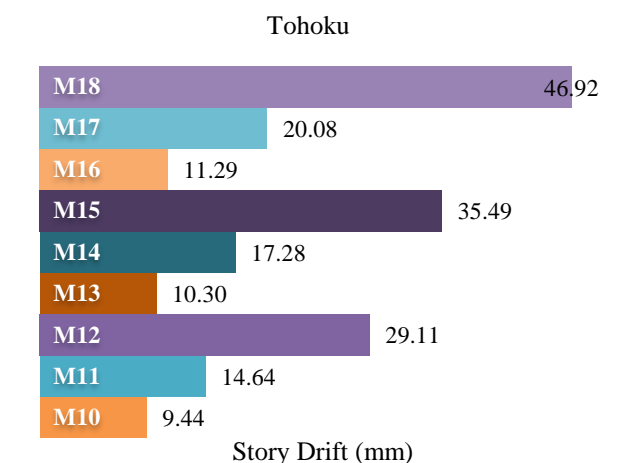


Figure 28. The story drift for model B (Tohoku)

Figure 26-28 indicates that increasing the L/H ratio significantly amplifies the story drift (δ), thereby impacting structural stability. For comparative analysis under the Coyote earthquake, Models M10, M11, and M12-each with a rafter angle of 10° but varying L/H ratios of 1, 1.5, and 2, respectively—were examined. Model M10 exhibits a story drift (δ) of 9.59 mm, while Model M11 shows 17.04 mm, reflecting a 77.68% increase. Model M12 records 29.68 mm, marking a 209.48% increase from Model M10. Rafter angle variations negligible impact on story drift (δ). For instance, Models M10, M13, and M16 were analyzed under the Coyote earthquake. All share an L/H ratio of 1 with rafter angles of 10°, 15°, and 20°, respectively. Model M10 exhibits a story drift (δ) of 9.59 mm, Model M13 at 10.33 mm (a 7.72% increase from M10), and Model M16 at 11.41 mm (an 18.98% increase from M10). Although increased story drift (δ) can compromise structural stability, maintaining it within allowable limits is crucial. Section 2.4 identifies the allowable limit (Δa) as 200 mm. Models M10 through M18 maintain story drift (δ) values below this threshold, confirming the structural compliance of all Type B models.

Stability is achieved when the stability coefficient (Θ) remains below the allowable threshold (Θmax) .

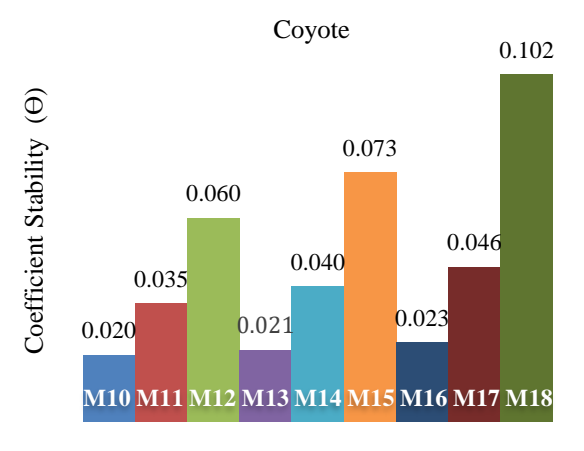


Figure 29. Coefficient Stability for model B (Coyote)

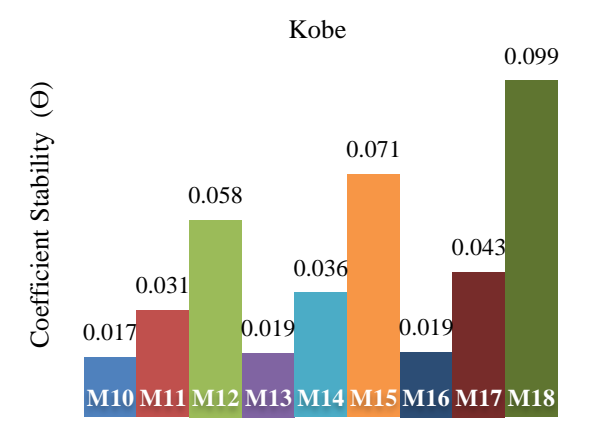


Figure 30. Coefficient Stability for model B (Kobe)

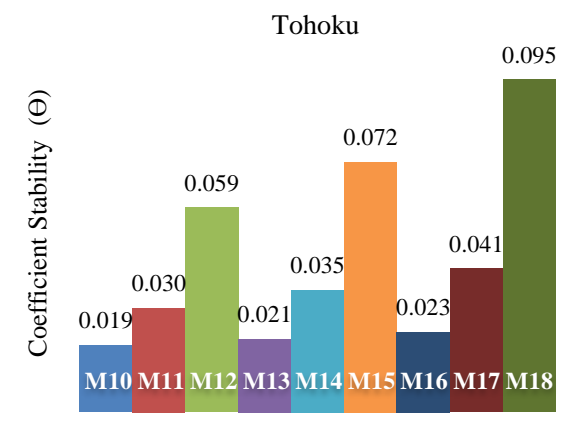


Figure 31. Coefficient Stability for model B (Tohoku)

Based on figure 29-31, all models from M10 to M18 exhibit stability across all three seismic scenarios, as their stability coefficients (Θ) remain below the maximum allowable threshold (Omax) of 0.167. The stability coefficients follow the trend M12 > M11 > M10, indicating that increasing the L/H ratio significantly enhances structural stability, which aligns with the story drift (δ) analysis results. For example, under the Coyote earthquake data, M10 has a stability coefficient (Θ) of 0.019, M11 has 0.030 (a 57.89% increase from M10), and M12 reaches 0.059 (a 210.53% increase from M10). While the L/H ratio has a notable impact on stability, the rafter angle shows minimal influence. Specifically, M10 with a 10° rafter angle has a stability coefficient of 0.019, M13 with a 15° angle has 0.021 (a 10.53% increase from M10), and M16 with a 20° angle has 0.023 (a 21.05% increase from M10). This trend is consistent with the story drift (δ) results for models M10 to M18, where increasing story drift (δ) leads to higher stability coefficients (Θ) , indicating structural instability. Both story drift (δ) and stability coefficients (Θ) are influenced by structural stiffness. Modal analysis using SAP 2000 shows that M10 has a stiffness of 264.89 kN/m, M11 has 222.35 kN/m, and M12 has 192.67 kN/m. Thus, increasing the L/H ratio reduces stiffness, resulting in higher story drift (δ) and stability coefficients (Θ), ultimately decreasing structural stability.

The following are the ductility values for the structures in model B.

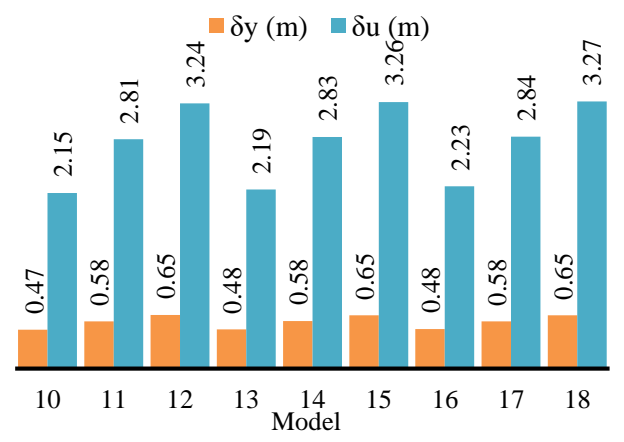


Figure 32. Yield and ultimate displacement for model B Daktilitas

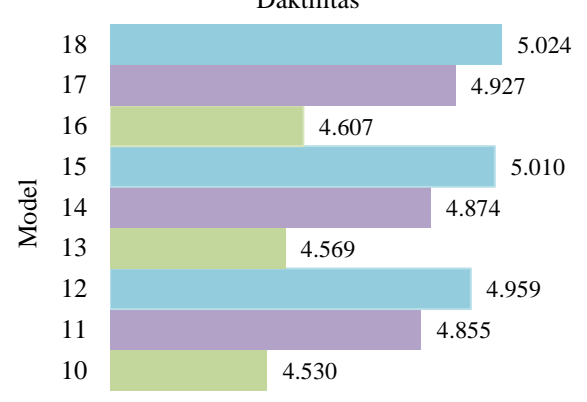


Figure 33. The ductility of model B

As shown in Figure 33, models M10 to M18 exhibit ductility values ranging from 4.5 to 6.0, classifying all type B models as Intermediate Moment Frames (IMF). Ductility progressively improves in models M10, M11, and M12. These models share a rafter angle of 10° but differ in L/H ratios of 1, 1½, and 2, respectively. Model M10 exhibits a ductility value of 4.530, M11 shows 4.855 (a 7.17% increase), and M12 has 4.959 (a 9.47% increase). For models M10, M13, and M16, the increase in ductility is marginal. With the same L/H ratio of 1 but varying rafter angles of 10°, 15°, and 20°, model M10 has 4.530, M13 has 4.569 (a 0.86% increase), and M16 has 4.590 (a 1.32% increase). Although increasing the rafter angle slightly enhances ductility, the effect is minimal.

C. Comparison between Model A and Model B.

Type A models, ranging from M1 to M9, utilize ductile sections, while type B models, from M10 to M18, employ non-ductile sections.

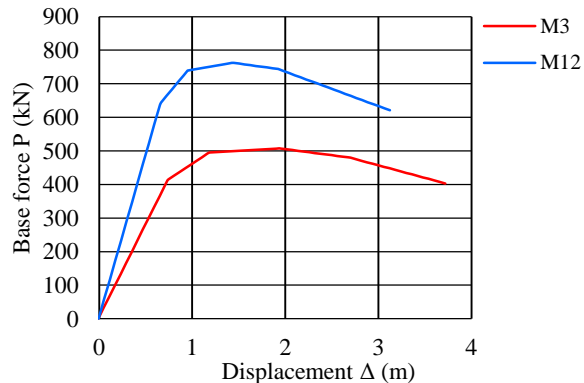


Figure 34. The pushover curves for M3 and M12

Models M3 and M12, both with an L/H ratio of 2 and a rafter angle of 10°, differ in profile sections. M3 utilizes a ductile section (column – HB 300, rafter – WF 300x200), while M12 employs a non-ductile profile (column - HB 350, rafter – WF 350x250). Type A models, such as M3, have smaller cross-sectional areas for both columns (13,480 mm²) and rafters (7,238 mm²) compared to type B models, like M12, with columns (17,390 mm²) and rafters (8,815 mm²). As a result, type B models are heavier and stiffer, which influences the structure's ductility and stability. Figure 12 demonstrates that model M3 is more ductile than model M12, with M3 exhibiting a ductility value of 5.069 and M12 showing a value of 4.959, a 2.17% decrease. The significant difference, however, is observed in the ultimate displacement (Δu), where M3 has $\Delta u = 3.72$ m, and M12 has $\Delta u = 3.24$ m, a 12.90% decrease. M3 also shows superior elastic behaviour, with a yield displacement (Δy) of 0.73 m, compared to M12's Δy of 0.65 m, reflecting a 10.96% reduction.

The reduced ductility, Δu , and Δy in M12 are attributed to its non-ductile profile, whereas M3's lower stiffness (128.29 kN/m) results in greater flexibility and larger plastic deformations, as seen in the pushover graph in Figure 12. However, a decrease in structural stiffness must be managed to avoid excessive flexibility that could lead to instability. Therefore, values for story drift (δ) and the stiffness coefficient (Θ) are monitored. The higher stiffness of M12 results in lower ductility compared to M3, but its increased stiffness negatively impacts story drift and stability. For instance, in the Coyote earthquake data, M3 exhibits a larger story drift (46.77 mm) and stability coefficient (0.106) compared to M12, which shows 29.68 mm of story drift and a stability coefficient of 0.060. This indicates that M3, being more flexible, exhibits more ductile behaviour than M12.

CONCLUSIONS

Based on the preceding explanation, the following conclusions can be inferred:

- Increasing the span length in warehouse frames significantly enhances structural ductility but compromises stability due to increased flexibility, resulting in greater plastic deformation, as evidenced by the pushover curve. The reduction in structural stiffness requires careful management to prevent excessive flexibility and potential instability. Thus, controlling story drift (δ) and the stability coefficient (Θ) within permissible limits is essential to maintain structural safety.
- 2. Increasing the rafter angle has minimal impact on structural ductility and stability because the structural stiffness remains largely unchanged.
- 3. Structural stiffness significantly impacts the ductility and stability of warehouse frames. For example, in model M3 (structural stiffness 128,29 kN/m) exhibits greater ductility and flexibility than M12 (structural stiffness 192,67 kN/m) due to its ductile section and lower stiffness, resulting in higher ultimate and yield displacements. However, this flexibility increases story drift and the stability coefficient, highlighting a tradeoff between ductility and stability. Proper control of stiffness, story drift, and stability is crucial to



- maintaining structural performance under seismic loading.
- 4. For optimal seismic performance in warehouse frames, a balanced structural configuration is recommended, involving moderate span lengths and the use of ductile sections with controlled stiffness. While increased ductility enhances energy dissipation capacity, excessive flexibility can adversely affect structural stability. Therefore, maintaining structural stiffness within an intermediate range, along with controlling story drift (δ) and the stability coefficient (Θ) within permissible limits, is essential to achieve an effective balance between ductility and stability in practical applications.

ACKNOWLEDGMENTS

The authors extend his sincere appreciation to his supervisor, Budi Suswanto, S.T., M.T., Ph.D., and Dr.Eng. Aniendhita Rizki Amalia, S.T., M.T., for their exceptional guidance, insightful feedback, and unwavering support throughout this research. Their expertise and mentorship were pivotal in the development and completion of this research.

REFERENCES

- [1] Kumar, Design of Steel Structures II. 2018.
- [2] H. Goel and R. Kumar, "Design and Analysis of Framed Steel Structure for Warehouse," 2021.
- [3] A. Ghasemof and M. Mirtaher, "A multi-objective optimization framework for optimally designing steel moment frame structures under multiple seismic excitations," Techno-Press, vol. Vol. 23, No. 1 (2022) 035-057, 2022, [Online]. Available: http://www.techno
 - press.com/journals/eas&subpage=7
- [4] Gandy, Carbon Steel Handbook. 2007.
- [5] B. Gao et al., "Enhanced strength and ductility of the low-carbon steel with heterogeneous lamellar dualphase structure produced by cyclic intercritical rolling," J. Mater. Res. Technol., vol. 23, pp. 6230– 6243, Mar. 2023, doi: 10.1016/j.jmrt.2023.02.214.
- [6] E. Arifi, Perencanaan Struktur Baja Berdasarkan SNI 1729:2020. 2020.
- [7] M. Soori and F. K. G. Jough, "Artificial Intelligent in Optimization of Steel Moment Frame Structures: A Review," World Acad. Sci. Eng. Technol. Int. J. Struct. Constr. Eng., vol. Vol:18, No:3, 2024, pp. 141–158, 2024.
- [8] N. Lisperguier, Á. López, and J. C. Vielma, "Seismic Performance Assessment of a Moment-Resisting Frame Steel Warehouse Provided with Overhead Crane," Materials, vol. 16, no. 7, p. 2815, Mar. 2023, doi: 10.3390/ma16072815.
- [9] X. Chun Liu and X. Wu Liu, "Seismic performance of recentering energy dissipation bracing with pendulum in prefabricated steel frame structure systems," Sci. Direct, 2024, [Online]. Available: https://www.elsevier.com/locate/jcsr
- [10] R. Y. Liu and Y. Z. Zhu, "Behavior of the damage-tolerant beam-column connection for earthquake-resilient steel frame: Experimental and numerical study," 2024.

- [11] J. H. Ling, Y. T. Lim, and E. Jusli, "Methods to Determine Ductility of Structural Members: A Review," J. Civ. Eng. Forum, pp. 181–194, May 2023, doi: 10.22146/jcef.6631.
- [12] B. Gao, L. Wang, and Y. Liu, "High-strength, high-ductility low-carbon steels are critically needed to facilitate structural lightweighting and enhance overall structural safety.," Elsevier, 2024, [Online]. Available: www.elsevier.com/locate/jmrt
- [13] M. Bruneau, C.-M. Uang, and A. Whittaker, Ductile design of steel structures, 2nd ed. New York: McGraw-Hill, 2011.
- [14] M. A. Faizy and S. B. B. Aval, "Seismic behavior of a novel slotted steel plate shear wall under monotonic, cyclic, and time history analysis," Elsevier, 2023, [Online]. Available: https://www.elsevier.com/locate/structures
- [15] R. A. Tamboli, Handbook of Structural Steel Connection Design and Details, Third Edition. 2017.
- [16] S. Benedetto and A. B. Francavilla, "Seismic behaviour of a steel moment resisting frame structure featuring hourglass double split tee joints," 2024.
- [17] AISC 341-16, "Seismic Provisions for Structural Steel Buildings." 2016.
- [18] AISC 360-16, "Specification for Structural Steel Buildings." 2016.
- [19] H. Slack and F. Walport, "A consistent approach to the definition of initial geometric imperfections for in-plane stability design of steel moment frames," Elsevier, 2024, [Online]. Available: www.elsevier.com/locate/structures
- [20] L. yi Yang and M. Ye, "Seismic performance of steel frame structures equipped with novel displacement-amplified friction dampers," Sci. Direct, 2024.
- [21] S. Jahanpanahi and I. Shamim, "The task of strengthening existing structures in high seismicity regions, particularly those prone to weak performance during strong ground motions, presents a significant challenge to design engineers," KSCE J. Civ. Eng., 2024.
- [22] L. Possidente and F. Freddi, "Dynamic increase factors for progressive collapse analysis of steel structures considering column buckling," Elsevier, 2024, [Online]. Available: https://www.elsevier.com/locate/engfailanal
- [23] S. Ibanez and M. Kraus, "Numerical method for the primary torsional capacity of arbitrary steel cross sections considering nonlinear plastic behaviour," Elsevier, 2024, [Online]. Available: https://www.sciencedirect.com/journal/results-inengineering
- [24] H. N. Hu and H. truong Viet, "Machine Learning-based prediction of seismic lateral deflection of steel trusses using nonlinear time-history analysis," Elsevier, 2024.
- [25] A. S. Patil and P. D. Kumbhar, "Time History Analysis of Multistoried RCC Buildings for Different Seismic Intensities," 2013.
- [26] N. G. Leiva and R. A. Herrera, "Numerical modeling of beam plastic hinges in steel moment resisting frames including local buckling and stiffness/strength degradation," Sci. Direct, 2024,



- [Online]. Available: https://doi.org/10.1016/j.istruc.2024.107260
- [27] M. Liapopoulou and P. J. Stafford, "Duration-dependent seismic collapse capacity prediction for steel moment resisting frames," Elsevier, 2024, [Online]. Available: https://www.elsevier.com/locate/jobe
- [28] N. D. Lagaros, C. Ch. Mitropoulou, and M. Papadrakakis, "Time History Seismic Analysis," in Encyclopedia of Earthquake Engineering, M. Beer, I. A. Kougioumtzoglou, E. Patelli, and I. S.-K. Au, Eds., Berlin, Heidelberg: Springer Berlin Heidelberg, 2013, pp. 1–19. doi: 10.1007/978-3-642-36197-5_134-1.
- [29] M. C. Perez, "Limit analysis of planar steel frames, in-element plastic-hinge for uniformly distributed loads," Sci. Direct, 2024, [Online]. Available: https://doi.org/10.1016/j.ijnonlinmec.2024.104827
- [30] L. K. Aswini, "Pushover analysis A Review," vol. 11, 2024, [Online]. Available: https://www.researchgate.net/
- [31] Q. T. Yi and Z. He, "A novel efficient plastic hinge approach for direct analysis of steel structures," 2024, [Online]. Available: https://www.elsevier.com/locate/engstruct
- [32] G. S. Patil and D. M. B. Chougule, "159 Warehouse Design," 2020.
- [33] Alan Scott Hoback and Naser Katanbafnezhad, "Optimum roof angles of steel gable frames with pinned supports." 2020.
- [34] ASCE 7-22, "Minimum Design Loads and Associated Criteria for Buildingsand Other Structures." 2022.